A Haptic Simulator for Studying Rest-To-Rest Reaching Movements in Dynamic Environments

Igor Goncharenko
3D Incorporated
2-3-8 Shin-Yokohama
222-0033, Yokohama, Japan
igor@ddd.co.jp

Mikhail Svinin
Kyushu University
744 Motooka, Nishi-ku,
819-0395, Fukuoka, Japan
svinin@mech.kyushu-u.ac.jp

ABSTRACT

We present a haptic simulation system with interchangeable physical constraints for studying skillful human movements. The unified haptic interface easily links different physical models with 2D and 3D static spatial constraints and graphical content related to the models. The system was tested on a variety of reaching tasks performed by human subjects. In the experiments, we analyzed motions based on data recorded by a history unit with a frequency of 100Hz. Theoretical and experimental kinematic profiles were compared for several cases of basic reaching rest-to- rest tasks, namely, line-constrained movement during transport of flexible object and parallel flexible object. Experimental patterns exhibit a good agreement with theoretical optimal control models based on jerk and force-change minimization criteria.

Keywords

Haptic interface, rest-to-rest movement, dynamic environment, optimality

1. INTRODUCTION

Numerous haptic applications have demonstrated subjectively realistic modeling of kinesthetic and tactile sensations of virtual reality (VR) object properties as such as mass, inertia, shape, viscosity friction, vibration, stiffness, and roughness. Many of these applications deal with *constrained* human movements, but little is known about movement formation in the constrained real and virtual environments (VE). In addition to practical (e.g., VR rehabilitation [Bur03]) and entertainment applications, simulators can be used for basic research in computational neuroscience (CN) studying movement trajectory formation and invariant features of movements.

Consider, for instance, point-to-point and rest-to-rest reaching tasks, typical in VR rehabilitation [Pir03]. If a static three-dimensional (3D) surface- or curve-based constraint, e.g., an ellipsoid, or a circle, is used in a haptic system as a VR constraint, the user's hand trajectories follow the specified 3D curve or lie on the surface. In CN research, unconstrained reaching exhibits invariant features as such as low curvature and bell-shaped velocity profiles. Invariant features change when movements are constrained by curves or surfaces. We do not, however, know how specifically they change or how change is related to constraint geometry and human visual feedback.

To clarify the problem of constraint hand movement formation in rest-to-rest reaching tasks, this paper presents an analysis of human movements in manipulation of flexible objects. This analysis is based on experiments completed with a haptic simulator.

Related works

Developing mathematical models and optimality criteria for predicting human movements constrained by the environment remains an open research area in CN. Some criteria [Fla85, Fla03, Uno89, Svi04a, Din04, Lei12, Mor95] are given in **Table 1**. In optimization approaches, the trajectory of the human arm is found by minimizing, over movement time T, integral performance index J subject to boundary conditions imposed on start and end points. In **Table 1**, x is the hand contact point vector, f is the force applied to the end point, τ is the vector of arm joint torques, and x_{cm} is the center of mass (CoM) of the system "hand-object". (Note, that superscript (5) in **Eq. (3)** means the 5th derivative.)

Minimum jerk is commonly accepted criterion in CN. However, numerous experiments of hand movement capturing in haptic environments were done by using simple "one mass – one spring" dynamic object model. For such a simple model, hand and object movement trajectories predicted by

different criteria may be very similar. In some cases [Lei12], the minimum hand jerk criterion is rejected as not applicable. To correctly discriminate the criteria, hand movement should be studied by interaction with complex dynamic environment , like multiple mass-spring objects. Right selection of optimality criterion is important for such areas as robotics, computer animation, CN, biological cybernetics.

The advent of haptic technology is making it possible to confirm or disapprove movement prediction criteria because potentially any type of VR constraint may be implemented in systems. Typically, haptic interaction is simulated using collision detection, often accelerated by GPU-based calculations (e.g., [Kal14, Vei09, Wel11]). As human rest-to-rest movements are smooth, we do not use collision detection, but utilize smooth analytical constraints (with smooth derivatives), which are parametric curves and surfaces in 3D space. In this case, object - constrained dynamic integration is very fast and does not require any parallelism, or separate threading of simulation. To do so, we built a haptic visualization environment. During design, we first required that constraints should be easily interchangeable and linked to the physical simulator core to study human arm movements in different constrained VEs.

Criterion name	Performance index	Ref
Minimum jerk	$J = \int_0^T \dddot{x}^T \dddot{x}\, dt$	(1)
Minimum joint torque change	$J = \int_0^T \dot{\tau}^T \dot{\tau}\, dt$	(2)
Minimum crackle	$J = \int_0^T x^{(5)T} x^{(5)}\, dt$	(3)
Minimum hand force	$J = \int_0^T f^T f\, dt$	(4)
Minimum hand force change	$J = \int_0^T \dot{f}^T \dot{f}\, dt$	(5)
Minimum CoM acceleration	$J = \int_0^T \ddot{x}_{cm}^2\, dt$	(6)

Table 1. Optimality criteria for movement prediction.

There are three novel aspects considered in this paper:

- Usage of changeable analytical constraints in haptic simulators instead of collision detection;
- Modeling of dynamic environment as flexible objects, namely, multiple mass-springs connected in sequential or parallel manner and following the spatial constraints;
- Usage of the proposed simulator in experiments to approve human hand rest-to-rest motion planning strategy in accordance with the minimum jerk / minimum hand force change optimization criteria.

Section 2 discusses the distributed architecture connected single point force devices via networks to study cooperative and collaborative arm movements. Section 3 describes the use of changeable spatial constraints in the physical-based simulation module. Note, that the method of constraint generation calculates not only dynamic coefficients, but also coordinates of curve/surface in 3D. This can be instructive for graphics community specialized in parametric curve/surface modeling and rendering. Sections 4-5 demonstrate controlling flexible VR objects. These sections compare collected haptic experimental data with theoretical optimality criteria. Section 6 presents conclusions.

2. HAPTIC SYSTEM DESIGN

We built our system (**Fig.1**) based on two dual-CPU PCs (server and client), interconnected via Ethernet, and each equipped with its own point force device.

Industry-standard PHANToM devices originally developed at MIT [Sal97] are suitable for studying constrained human movement. In our case, SensAble/Geomagic PHANToM 1.5/6.0, PHANToM High Force, and Omni manipulators controlled through Open Haptic Toolkit [Geo] were used. Critical loops in the overall control scheme include haptic rendering, graphical rendering, and a simulation loop. We focused on the efficiency of haptic and simulation loops to achieve real-time capabilities and robust realistic interaction via point-force devices in constrained VEs.

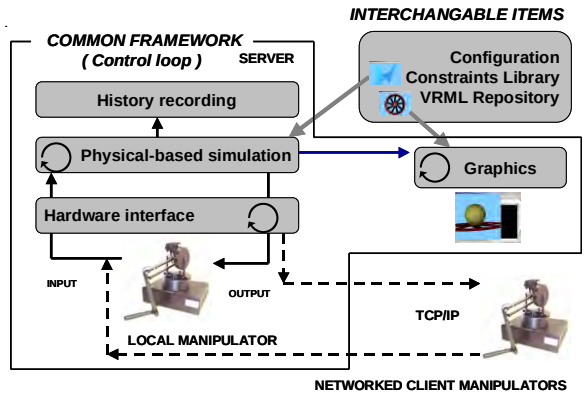

Figure 1. System architecture.

To support haptic simulator cloning, new dynamic models are reduced to the following standard *N*

ordinary differential equations (ODE) with *M* time-dependent parameters:

$$dy_i / dt = f_i(y_{1,}...y_{N,}c_1(t),...,c_M(t)) \quad , (7)$$

where parameters $c_i(t)$ ($1 \le i \le M$) are control functions. Different constraints f_i are linked to the physical simulator from the external constraint library. During simulation, system (7) is integrated by the Runge-Kutta 4th-order method for the time step 0.001s, defined by the constant haptic cycle of PHANToM devices. Typically, controls $c_i(t)$ are feedback force and moment components. To calculate feedback, we introduced a fixed point (FP) for Hooke's and spring-damper models [Bur03]. At the start of haptic interaction, FP is coincided with haptic interface point (HIP, or proxy), and it is considered as rigidly bound to the VR body during simulation. Distance $\Delta r(t)$ between current HIP and FP defines force $F(t)$ applied to the VR body:

$$F(t) = k_h \Delta r(t) + b_h \Delta \frac{dr(t)}{dt} \ , \qquad (8)$$

where k_h, b_h are coefficients of the spring-damper model.

Force components of (8) are used in **Eq.(7)**, and generated haptic feedback force is just opposite to the force given in **Eq.(8)**. In constrained VEs, this models human movements such as hook-and-carry and catch-and-move.

The history unit records all simulation data: time-dependent parameters, feedbacks, object and hand positions, velocities and accelerations. Recording is performed at a frequency of 100Hz, sufficient to analyze basic human motions with the average reaction time above 200ms. The system required certain flexibility in different constraints, attained by developing two additional parts – a configuration repository and a constraints library. The configuration module defines initial dynamics model values, graphical scene representation (references to VRML scenes), and static parameters such as mass, inertia, and viscosity friction. VRML objects are completely independent and are replaced in the configuration repository.

Constraint types and shapes are defined analytically in the constraints library. For parametric surface- and curve-constraints, we developed a partially semiautomatic procedure to generate functions f_i (7). A general library written in Mathematica [Wol03] is processed, with each surface/curve type in this library defined in a simple analytical form by surface/curve radius-vector components. Partial derivatives of the radius-vector and necessary dynamics coefficients (Section 3) are calculated as analytical expressions, which are exported in C-code by Mathematica, compiled, and linked to an ODE solver to be used in the simulation loop.

Several haptic devices (clients) connected to the server via Ethernet had to be supported to study two-hand cooperative and multi user collaborative movements (e.g., [Gon04]). **Fig.1** demonstrates the simplest client-server configuration. In this research, only one manipulator is used.

As the number of ODEs is very small for curve/surface constraints and right parts of equations (7) can be expressed in analytical form, one time step integration of ODEs to calculate dynamic environment (in case of mass-spring connections, positions of the centers of masses) is negligible in comparison with the haptic cycle (0.001s). That is, physical simulation (**Fig**.1) can be implemented directly in the haptic thread. Therefore, a simulator similar to the described one can be implemented as two-thread CPU-based application. In this case, the graphical rendering thread gets positions of masses calculated in the haptic thread. Functionality of the haptic thread is straightforward: the thread receives HIP position, calculates object driven force (and, haptic force as opposite to the driven force) by (8), calculates right parts of equations (7), performs integration by the Runge-Kutta method for the time step 0.001s (correspondent to the haptic cycle) to get positions of masses, and, finally, applies haptic forces to the haptic device. In the above calculation scheme, subject's rest-to-rest movement trials are realized as follows. When dynamic system is at the start position, driven/haptic forces, masses' accelerations and velocities are zeroed, that is the dynamic system is at rest. A movement trial starts by application of non-zero forces (8) and continuous integration is performed. When the system reaches the target position (with some tolerances on velocities/accelerations), the forces are zeroed again. When a signal to proceed with the next trial appears, the system is placed to the rest start position, and so on.

3. MODELING OF CONSTRAINTS

Different 2D and 3D constraints are derived, reduced to form **Eq.(7)** and linked to the simulator. Movements are assumed applied to VR objects via a single haptic interface. Realistic rigid body (or, flexible object) sensations are achieved when stiffness coefficients (k_h in **Eq.(8)**) for feedback exceed 500N/m. For such values, force damping and clamping may be required for fast movements because PHANToM's maximum apparatus load is 12N (37N for PHANToM High Force). During the

course of our experiments, we configured the system to avoid exceeding of the force limits.

Consider a point of mass m in viscosity field λ. Assume that the point is loaded by external force $f = (f_x, f_y, f_z)^T$. Unconstrained dynamics are defined by

$$m\ddot{r} + \lambda\dot{r} = f \quad , \tag{9}$$

where $r = (x, y, z)^T$ is the radius-vector of the point. Assume now that the point is constrained by a 3D curve. The constraint curve is given by

$$r(\varphi) = \big(x(\varphi), y(\varphi), z(\varphi)\big)^T \tag{10}$$

for $\varphi \in [0, 2\pi]$.

Differentiating **Eq.(10)** and defining $\omega \equiv \dot{\varphi}$, the physical model of curve-restricted motions is then described by the following two first-order ODEs:

$$\dot{\varphi} = \omega,\ M(\varphi)\dot{\omega} + L(\varphi)\omega + V(\varphi)\omega^2 = r_\varphi^T f \ , \tag{11}$$

where

$$M = m\big(r_\varphi^T r_\varphi\big), L = \lambda\big(r_\varphi^T r_\varphi\big), V = m\big(r_\varphi^T r_{\varphi\varphi}\big),$$
$$r_\varphi \triangleq \frac{\partial r}{\partial \varphi} \ , r_{\varphi\varphi} \triangleq \frac{\partial^2 r}{\partial \varphi^2} \ .$$

Dynamic equations (11) now match the form (7) and are used for the simulator. Such model parameters as mass of point m and viscosity coefficient λ are defined in the configuration repository.

By analogy, equations for surface constraints are derived using **Eq.(9)** and assuming that movements are constrained by the (u,v)-parametric surface:

$$r(u, v) = \big(x(u, v), y(u, v), z(u, v)\big)^T \quad . \tag{12}$$

After finding derivatives of r, equations of the constrained system in coordinates (u,v) are:

$$mA(u, v)\begin{pmatrix}\ddot{u}\\ \ddot{v}\end{pmatrix} + \lambda B(u, v)\begin{pmatrix}\dot{u}\\ \dot{v}\end{pmatrix} + mC(u, v, \dot{u}, \dot{v}) = Q(u, v, f) \quad . \tag{13}$$

Elements of matrices A, B, and vectors C, Q depend on partial derivatives of radius-vector r by u and v and are found analytically. Equations (13) are rewritten as four first-order ODEs to fit form (7). The above analytical calculations are done automatically, and only basic curve/surface expressions (10) and (12) are needed to be defined. Note, that parameters u,v, φ are non-dimensional.

As an example, consider step by step the automatic constraint generation for task (11). Initially, two standard wrapping C-code patterns without calculation expressions (heads or tails) are created: the first one is used to interface dynamic constraints with a module solving ODEs (7), while the second one links curve coordinate calculations with a 3D graphical rendering module. The following unified script in Mathematica is then run:

```
(* VARIABLE PART: Curve definition *)
   Curve3d[a_,b_][fi_]:={0,aCos[fi] , bSin[fi]};
(* COMMON PART *)
(* Input forces and radius-vector*)
   f={fx,fy,fz} ;  r=Curve3d[a,b][fi];
(* Output coordinates of this 3D-curve *)
   x=r[[1]]; y=r[[2]]; z=r[[3]];
(* Derivatives *)
   rfi=Simplify[D[r,fi]]; dxdfi=rfi[[1]]; dydfi=rfi[[2]];
   dzdfi=rfi[[3]]; rfifi=Simplify[D[rfi,fi]];
(*  Coefficients of the dynamic equations  *)
    M=m Simplify[rfi.rfi];
    L=lambda Simplify[rfi.rfi];
    V=m Simplify[rfi.rfifi]; Q=Simplify[rfi.f];
(*Generate C- code  *)
    StringForm
    [
    "/*---------- Curve coordinates --------*/\n
    x = ``;\n   y = ``;\n   z = ``;\n
    /*---------- Dynamic parameters -------*/\n
    M = ``;\n  L = ``;\n   V = ``;\n  Q = ``;\n
    /*---------- END OF C-CODES -----------*/\n",
    CForm[x],   CForm[y],   CForm[z], CForm[M],
    CForm[L],   CForm[V], CForm[Q]
    ]
```

The script calculates analytically coordinates on the curve in 3D and dynamic parameters *M*, *L*, *V* given in formula (11). Operator "D" calculates partial derivatives, and operator "Simplify" fulfills analytical simplification (e.g., trigonometry, or algebra simplification). Operator "CForm" generates C-code to be used in haptic application. In the script, parts emphasized by bold font are variable. In this case, it represents a 3D ellipse. The expressions generated are automatically post-processed for further trigonometry optimization, merged with the wrapping patterns, compiled in batch mode, and added to the current constraint library.

Only simple analytical expressions, similar to the above one-line 3D ellipse definition, must be stored in and added to a source constraint library. At present, more than 30 such definitions are used for cloning haptic simulators with spatial constraints. GUIs with some of these constraints (epitrochoid, monkey saddle, plane, torus in 3D) are shown in

Fig.2. In the figure, small spheres represent start and stop positions for the driven object (larger sphere).

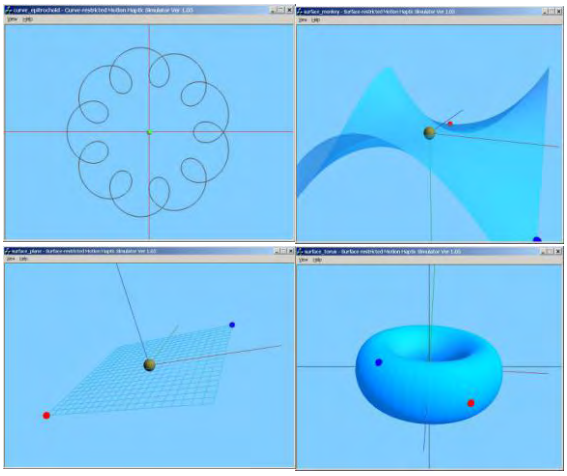

Figure 2. Curve- and surface-based constraints.

While conducting the requested point-to-point movement of the VR body, users can sense inertia of the driven object, the viscosity field, and the shape and curvature of the constraint surface. To control movement at arbitrary locations on surfaces, graphical rendering is done semi transparently or in a wire-frame. Haptic feedback is calculated using FP method (8).

Constraint changeability becomes very useful when a movement prediction criterion must be checked for a variety of constraint types. Below, we compare theoretical results based on different criteria (**Table 1**) with experimental data collected via the haptic system. For the experiments described in next sections the system was initially configured by selecting line constraint in 3D

$$r(\varphi) = \left(x_B + \frac{\varphi}{2\pi}(x_E - x_B)\right)^T, \qquad (14)$$

where $x_B = -0.1$ $x_E = 0.1$. These constants allow us to simulate constrained movement in haptic environment along horizontal line in the range of 20cm.

4. MOVEMENT OF FLEXIBLE OBJECTS

In addition to geometrically constrained movements, we also considered point-to-point rest-to-rest constrained movement for flexible objects, which may require long training and good skills from the system users. In [Din04], the simplest flexible VR system consists of a single mass, which humans can interact with through a haptic interface with a stiffness of 120N/m. We implemented multi mass system modeling to check hand movement optimality criteria. The flexible object (**Fig.3**) is modeled by several masses connected by damping springs, and external haptic force f_h is applied to the driving mass (right large sphere).

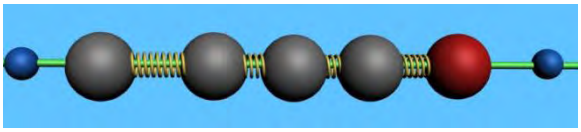

Figure 3. Flexible object model.

Masses move along a 3D curve and penetrate each other virtually, yielding very complex oscillation. Equations describing the flexible VR object for arbitrary 3D curve-constraint are derived, using formulas (9) for the case of N masses, so we have 2xN first-order ODEs:

$$\frac{d\varphi_i}{dt} = \omega_i, \quad 1 \le i \le N,$$
$$\frac{d\omega_i}{dt} = [r'^T_{\varphi_i}(\varphi_i) f_i - L(\varphi_i)\omega_i - V(m_i, \varphi_i)\omega_i^2] / M(m_i, \varphi_i),$$

where

$$f_i = k_{i-1}(r_{i-1} - r_i) + k_i(r_{i+1} - r_i) + b_{i-1}(\dot{r}_{i-1} - \dot{r}_i) + b_i(\dot{r}_{i+1} - \dot{r}_i) + g, \quad 1 < i < N$$
$$f_1 = k_1(r_2 - r_1) + b_1(\dot{r}_2 - \dot{r}_1) + f_h + g,$$
$$f_N = k_{N-1}(r_{N-1} - r_N) + b_{N-1}(\dot{r}_{N-1} - \dot{r}_N) + g.$$

g is the gravity acceleration, $f_h$is the external haptic force, $\dot{r} = \frac{\partial r}{\partial \varphi}\dot{\varphi}$, k_i, b_i are spring stiffness and damping coefficients. As derivatives of r found from (14) are constant, after setting λ=0 the above dynamic equations have classic Newton's law form. Prior to experiments, the system was configured to be constrained by a straight line. Gravity and line viscosity were set to zero. To be compatible with experimental results published by other researchers, all damping coefficients were also set to zero. Five equal 0.6kg masses are connected by springs (**Fig.3**) and all spring stiffness coefficients are equal to 600N/m. The PHANToM stiffness coefficient ($k_h$in (8)) is also 600N/m.

The reaching task was formulated for experimenters so that, initially, all masses are at rest and coincide at the initial point (small left sphere in **Fig.3**). Users were instructed to move the 5-mass system to the target point (small right sphere) during designated time T. All masses should finally be at rest and coincide at the target point. The travel distance was set to 0.2m. Tolerances were introduced to count successful reaching trials: position deviation, speed, and time tolerances $\Delta x, \Delta v, \Delta T$; and all masses must

obey the tolerances. When a reaching task is successful, haptic interaction is stopped and an audio signal prompts the user to proceed with the next trial.

Fig.4 schematically illustrates ergonomics of subjects during the experiments.

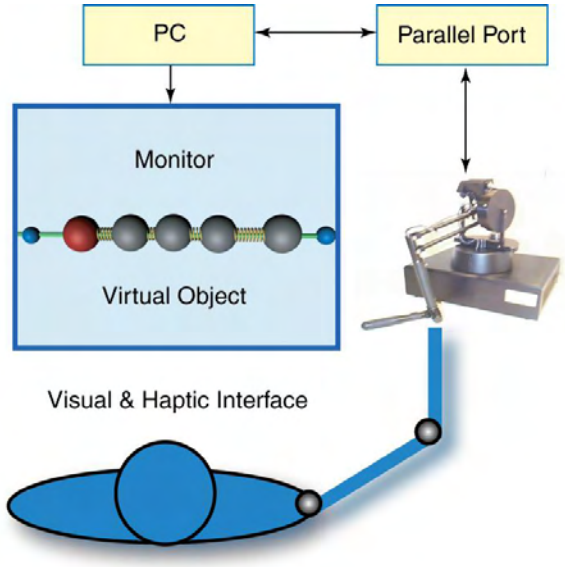

Figure 4. Experimental environment for movement of flexible object.

One subject conducted preliminary experiments and defined three tolerance sets at the subject's own pace for slow, moderate, and fast movements to make experimental results statistically representative. Procedure for defining the tolerance set for *moderate* movements is described below.

Reaching movements under consideration are quite unusual from what we experience in daily life movements, and an experiment – similar to [Din04] – was conducted in two days. On the first day, the subject was familiarized with the experimental setup, learned the unusual dynamic environment, and performed trial movements. Initially, the subject was asked to complete reaching during $T = 1.00 \pm 0.5\text{s}$ within tolerance windows $\Delta x = \pm 0.006\text{m}$, $\Delta v = \pm 0.006\text{m/s}$. It turned out that the learning of successful movements constituted only 5% of 100 trials. The low learning rate is attributed to the relatively narrow time, position, and velocity windows.

To facilitate learning, two windows were set as follows: $\Delta x = \pm 0.012\text{m}, \Delta v = \pm 0.012\text{m/s}$. On the 1st day the subject made 2 series of 100 trials, with overall success rate of about 10%. On the 2nd day the subject made 2 series of 100 trials, with overall success rate increasing to 17%. The average movement time become 1.35s (maximal 1.49s, minimal 1.13s, and standard deviation from average 0.09s). Similarly, slow and fast movement tolerances were as following :

Slow: $T = 2.26 \pm 0.5\text{s}$,
$\Delta x = \pm 0.006\text{m}, \Delta v = \pm 0.006\text{m/s}$;
Fast: $T = 0.68 \pm 0.5\text{s}$,
$\Delta x = \pm 0.012\text{m}, \Delta v = \pm 0.024\text{m/s}$.

Five subjects (4 men and one woman) participated in experiments based on the same scheme:

- All three tolerance sets were fixed as described above;
- On the first day, subjects made 100 preliminary trials for each slow, moderate, and fast movement task;
- On the second day, subjects made 100 additional trials for each slow, moderate, and fast movement task.

All experimental sets for all subjects demonstrated very similar results in favor of the minimum jerk criterion (1). Here, only the results for reaching time $T = 1.35\text{s}$ for one subject are shown.

Experimental velocity profiles, time-scaled to the average, are shown in **Figs.5** and **6** by thin lines. Hand and object velocity profiles, predicted by criteria (1) and (3) for constraints (12), are shown by thick solid and thick dashed lines, respectively. Note that the last fifth mass's velocity is given as "object velocity."

Experimental data favors the minimum hand jerk criterion. Experiments with one mass of 3kg and PHANToM's stiffness equal to 120N/m were also conducted to check results reported in [Din04]. For this configuration, predicted velocity profiles are very close in magnitude and shape for both (1) and (3) criteria. In [Svi04b, Svi06] it was proved that the minimum crackle criterion does not converge to criteria (1) when stiffness is increased. When number of masses N is increased, the criterion (3) gives unconstrained velocity profiles, asymptotically approaching the Dirac delta function.

All subjects showed progress in motor training from Day 1 to Day 2 (D1, D2 in **Table 2**). Note that subject S1 established tolerance first for moderate, then for fast, then for slow movement, i.e., participating in 6 experiments. Subject S2 volunteered on two additional days, making 2 sets of experiments daily for each of the movements. In the table, S, M, and F mean slow, moderate and fast movements.

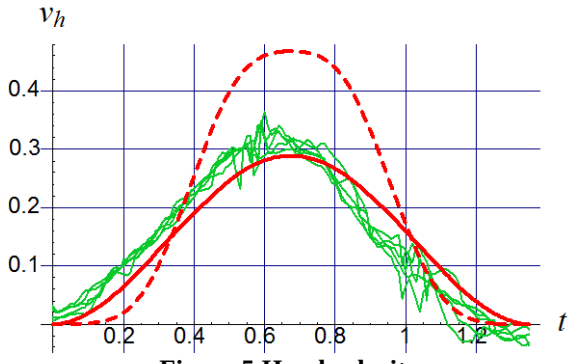

Figure 5 Hand velocity

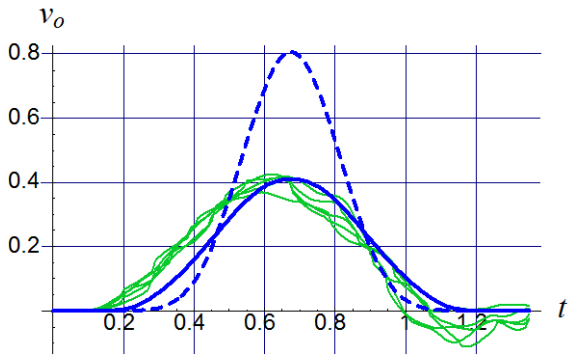

Figure 6 Object velocity

Subj	S D1	S D2	M D1	M D2	F D1	F D2
S1	64	76	10	17	14	23
S2	17	36	31	44	17	31
S3	40	73	35	47	19	28
S4	46	93	41	82	20	51
S5	32	55	25	48	17	27

Table 2 Progress in motor learning (success, %)

5. PARALLEL FLEXIBLE OBJECTS

Studying of flexible objects transport in haptic environments was carried by several researches. However, the majority of experimental works deals with only one mass virtually "connected" to human hand via the haptic proxy. The advantage of our system is that it can simulate highly dynamic environment with several masses, connected by springs. After some configurations of the system, experimental data can be collected to make choice in favor of one of the criteria (1)-(6). Not only bell-shape velocity profiles can be observed; for instance, two- and three-phase profiles were observed, that match well to theoretical profiles [Svi06, Gon10].

Recently, a novel model, named as the minimum acceleration of the center of mass (6), has been proposed and tested against experimental data for a single mass flexible object [Lei12]. In the theoretical justification of this model it is argued that neither the minimum hand jerk model (1) nor its dynamic counter- part, the minimum hand force change model (5), are applicable to modeling of reaching movements with parallel flexible objects.

Contrary to the above statement, we demonstrated that the invariant features of hand trajectories in the manipulation of parallel flexible objects can be well captured by the minimum jerk hand model, and theoretical solution for 2-mass-hand system was found [Svi16].

From the standpoint of haptic dynamic simulation, change of haptic force is needed (spring model without damping):

$$F(t) = k_1(x_1 - x_h) + k_1(x_2 - x_h) \quad .$$

And, the motion equations are:

$$m_1\ddot{x_1} + k_1(x_1 - x_h) = 0,$$
$$m_2\ddot{x_2} + k_2(x_2 - x_h) = 0,$$

where m_1, m_2, k_1, k_2 , x_1, x_2 are masses, spring stiffness, and coordinates of first and second mass, and x_h is the hand coordinate (HIP). The above expressions were used to build a new constraint, which was added to the haptic simulator's solver.

In (**Fig.7**) light smaller sphere center is the human hand position, and small dark sphere is the target point. For visualization convenience, 2 driven masses are spatially shifted only for rendering, even physical simulation is done for driven masses that are moved along the same line (that is, they can virtually penetrate through each other). During the course of experiments, the line constraint is horizontal.

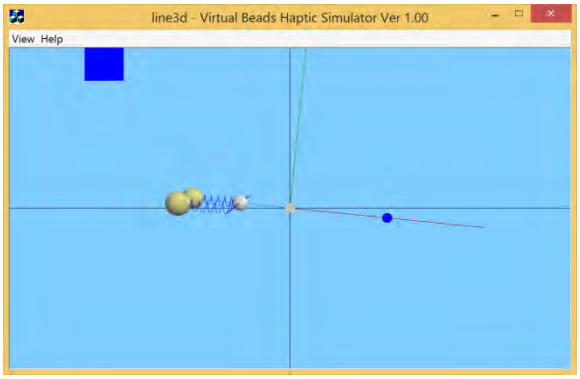

Figure 7. Haptic simulator interface for parallel flexible object.

The square near the top left corner of the GUI window is a semaphore. It provides visual feedback for better motor learning. When trial time is approaching to the described above reaching task time T (with the defined tolerances $\pm\Delta T$), color of the semaphore is changed to green, and if the trial time exceeds maximum $(T + \Delta T)$, color becomes red.

Fig.8 schematically illustrates ergonomics of subjects during the experiments.

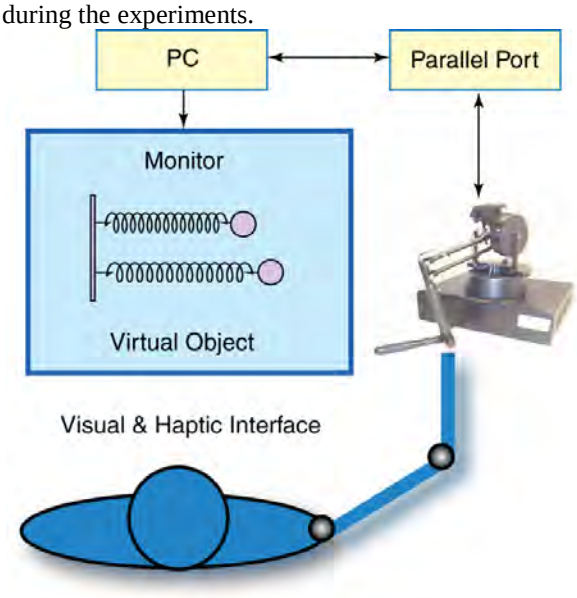

Figure 8. Experimental environment for movement of parallel flexible object.

The experiments were conducted similar to the experimental scheme presented in Section 4, with the following configuration:

$$m_1 = m_2 = 3\text{kg}, \; , k_1 = 50\text{N/m}, k_2 = 250\text{N/m} \; ,$$
$$T = 2.5 \pm 0.3\text{s}, \Delta x = \pm 0.012\text{m}, \Delta v = \pm 0.012\text{m/s}.$$

Fig.9 and **Fig.10** illustrate 5 last trials in experimental series for one of the subjects (thin lines). Thick grey line depicts theoretical velocity profile, and thick black line is the subject's average through all successful trials. Qualitatively, the experimental velocity patterns were similar to theoretically predicted by criterion (1). A quantitative measure for the comparisons was represented by the integrated RMS of the velocity errors,

$$\varepsilon = \sqrt{\frac{1}{N}\sum_{i=1}^{N}\left(v_{pred}(t_i) - v_{exp}(t_i)\right)^2} \quad ,$$

over the trajectories between the theoretical predictions and the experimental data. Here, N is the number of sampled data in one experimental series (only successful trials are considered). Similar RMS estimator was used for the experiments described in Section 4. Complete analytical solution derivation and experiment description is given in [Svi16].

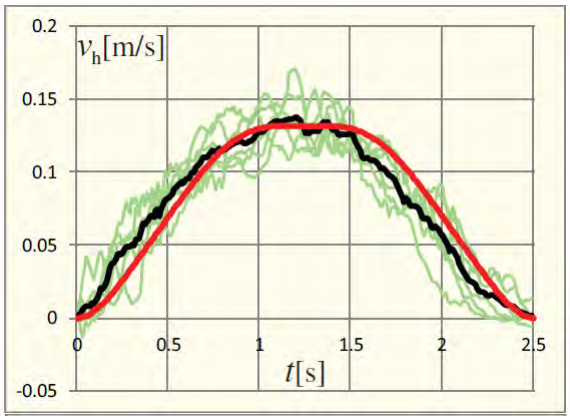

Figure 9. Hand velocity profiles.

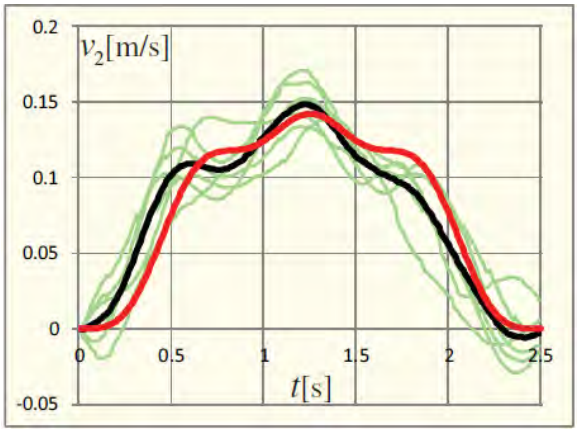

Figure 10. Object velocity profiles (mass 2).

6. CONCLUSIONS

We have discussed a real-time haptic system with interchangeable constraints. The interchangeability of constraints is achieved by a unified interface to link different physical models, basic constraints library processing, and external configuration of the models and associated graphical scenes. This property is required for studying basic constrained human movements, when theoretical movement prediction models should be checked with a large variety of constraints with different shapes, curvatures, viscosity, etc. Several criteria based on optimal trajectory planning were successfully studied with the system for line constraint in 3D for the task of rest-to-rest human movement during transport of flexible object and parallel flexible object.

Experimental data collected with the history unit are clearly in agreement with theoretical results based on the minimum jerk criterion and relating to it variations of the minimum hand force change criterion. This is indirect evidence of the fact that the

human central nervous system plans movements in the task space of hand coordinates. Theoretical velocity profiles correlate well with observed experimental data. Dealing with (parallel) flexible VR objects, subjects after training plan their control strategies to move flexible objects as "a whole", with hand velocity profiles restricted and bell-shaped..

The system facilitates the study of progress in motor movement skills training, when the convergence of hand trajectories to unique and finite profiles observed together with the increase in trial success.

7. REFERENCES

[Bur03] Burdea, G., and Coiffet, P. Virtual reality technology, 2nd Ed. Publ. Wiley-Interscience, 2003.

[Din04] Dingwell, J., Mah, C. F., and Mussa-Ivaldi, F. Experimentally confirmed mathematical model for human control of a non-rigid object. Journal of Neurophysiology, Vol.91, pp. 1158-1170, 2004.

[Fla85] Flash, T., and Hogan, N. The coordination of arm movements: An experimentally confirmed mathematical model. The Journal of Neuroscience, Vol.5, No.7, pp. 1688-1703, 1985.

[Fla03] Flash T., Hogan N., and Richardson M. Optimization principles in motor control. The Handbook of Brain Theory and Neural Networks, 2nd Ed. Arbib M. (ed.). Cambridge, Massachusetts, MIT Press, pp. 827–831, 2003.

[Geo] http://www.geomagic.com

[Gon04] Goncharenko, I., Svinin, M., et al. Cooperative control with haptic visualization in shared virtual environments. Proc. 8th IEEE Int. Conf. on Information Visualisation, London, UK, pp.533-538, July 14-16, 2004.

[Gon10] Goncharenko, I., Svinin, M., Hosoe, S., and Forstmann, S. On the influence of hand dynamics on motion planning of reaching movements in haptic environments. Advances in Haptics, In-Tech Publ., pp.451-462, 2010.

[Kal14] Kaluschke, M., Zimmermann, U., Danzer, M., Zachmann, G., and Weller, R. Massively-parallel proximity queries for point clouds. 11th Workshop on Virtual Reality Interaction and Physical Simulation, VRIPHYS, Bremen, Germany, pp. 19-28, September 24 - 25, 2014.

[Lei12] Leib, R., and Karniel, A. Minimum acceleration with constraints of center of mass: A unified model for arm movements and object manipulation. Journal of Neurophysiology, Vol. 108, No. 6, pp. 1646–1655, September 2012.

[Mor95] Morasso, P., and Sanguineti, V. Self-organizing body schema for motor planning. Journal of Motor Behavior, Vol. 27, No. 1, pp. 52–66, 1995.

[Pir03] Piron, L., Tonin, P., et al. A virtual-reality based motor tele-rehabilitation system. Proc. 2nd Int. Workshop on Virtual Rehabilitation, Rutgers Univ., pp. 21-26, September 21-22, 2003.

[Sal97] Salisbury, J.K., and Srinivasan, M.A. Phantom-based haptic interaction with virtual objects. IEEE Comput. Graph. Appl., Vol. 17, No. 5, pp. 6–10, 1997.

[Svi04a] Svinin, M., Odashima, T., Luo, Z., and Hosoe, S. On the optimization approaches to the trajectory formation of human movements. Proc. Int. Conf. on Complex Systems, Intelligence, and Modern Technology Applications, Cherbourg, France, pp. 628-633, September 19-22, 2004.

[Svi04b] Svinin, M., Masui, Y., Luo, Z., and Hosoe, S. On the dynamic version of the minimum hand jerk criterion. Proc. IEEE/RSJ Int. Conf. on Intelligent Robots and Systems, IROS2004, Sendai, Japan, Vol. 1, pp. 174-179, September 28-October 2, 2004.

[Svi06] Svinin, M., Goncharenko, I., Luo, Z., and Hosoe, S. Reaching movements in dynamic environments: How do we move flexible objects? IEEE Transactions on Robotics, Vol. 22, No. 4, pp. 724–739, 2006.

[Svi16] Svinin, M., Goncharenko, I., Lee, H., and Yamamoto, M. Modeling of human-like reaching movements in the manipulation of parallel flexible objects. IEEE/RSJ International Conference on Intelligent Robots and Systems (IROS 2016), submitted , 2016.

[Uno89] Uno, Y., Kawato, M., and Suzuki, R. Formation and control of optimal trajectory in human multi-joint arm movement: Minimum torque-change model. Biological Cybernetics, Vol. 61, pp. 89-101, 1989.

[Vei09] Veit, A. C. M., and Bechmann, D. Influence of degrees of freedom's manipulation on performances during orientation tasks in virtual reality environments. Proc. 16th ACM Symposium on Virtual Reality and Software Technology (VRST), pp. 51-58, Kyoto, Japan, November 18-20, 2009.

[Wel11] Weller, R., and Zachmann, G. 3-DOF vs. 6-DOF - Playful evaluation of complex haptic interactions. Proc. IEEE Int. Conf. on Consumer Electronics (ICCE), pp. 273-274, Las Vegas, NV, January 9-12, 2011.

[Wol03] Wolfram, S. The Mathematica Book, 5th Ed. Wolfram Media, 2003.